The Design and Function of α-Helix Rich, Heme Binding Peptide Materials

H. Christopher Fry*[1], Yuzi Liu[1] and Sunny K. Taylor[2]

1. Center for Nanoscale Materials, Argonne National Laboratory, 9700 S. Cass Ave. Lemont, IL 60439.

2. Pritzker School for Molecular Engineering, University of Chicago, 5640 S. Ellis Ave., Chicago, IL 60637

ABSTRACT: Peptide materials often employ short peptides that self-assemble into unique nanoscale architectures and have been employed across many fields relevant to medicine and energy. A majority of peptide materials are high in β-sheet, secondary structure content including heme binding peptide materials. In an effort to broaden the structural diversity of heme binding peptide materials, a small series of peptides were synthesized to explore the design criteria required for (1) folding into an α-helix structure, (2) assembling into a nanoscale material, (3) binding heme, and (4) demonstrating function similar to that of heme proteins. One peptide was identified to meet all four criteria including the heme protein function of CO binding and its microsecond to millisecond recombination rates as measured by transient absorption spectroscopy. Implications of new design criteria and peptide material function through heme incorporation are discussed.

INTRODUCTION

Self-assembled peptides represent a class of polymeric materials that are highly programmable due to the unique characteristics of each monomeric building block, the 20 canonical amino acids.[1-4] While success has been achieved in many areas like regenerative medicine, drug delivery,[5] and biosensing,[6] etc. there is also an excellent prospect for implementing peptide materials in addressing our worlds energy concerns.[7] Efforts towards a circular economy in developing new highly biodegradable materials,[8] selective capture of rare earth elements,[9] novel catalysts,[10] and solar energy conversion[11] represent a few of these

areas in which progress is being made. In order to afford functional peptide materials, one approach takes a cue from nature by incorporating chromophores with targeted functions.[11]

Heme proteins, for example, represent a large class of biomacromolecules that yield a massive variety of functions tailored by the surrounding protein.[12-14] Heme coordination occurs most commonly via nitrogen coordination from the imidazole ring of histidine. We have highlighted the engineering of histidine and bis-histidine binding sites in amphiphilic peptides that yield either micelles that exhibit random-coil secondary structure or fibrils rich in β-sheets.[15-17] The resulting structures presented unique properties imparted on the heme function by the nanoscale peptide assembly, e.g. the electronic properties and chiral arrangements of the chromophore.

While our findings identified many sequences and motifs in nanoscale architectures that bind heme, it should be noted that most heme molecules can be found coordinated in an α-helix rich protein environment.[12] Therefore, our curiosity has led us to design short peptides (16 amino acids in length) that self-assemble with an alpha-helical secondary structure and bind heme. While there are many examples of *de novo* designed helical bundles that bind heme and synthetic metalloporphyrins,[12, 14] and α-helix rich peptide assemblies,[18-20] there are few examples of self-assembling (i.e. forming nanoscale structures) peptides that are both rich in α-helices and capable of binding heme. Here, the design of the sequences will be described and supported by spectroscopic characterization detailing the assembly from the molecular to supramolecular scales. In addition, the function of the material will be highlighted by the assembly's ability to bind and release the small molecule carbon monoxide with emphasis on the ligand dynamics uncovered by transient absorption spectroscopy. Finally, future directions for this work will be discussed in terms of design and function.

MATERIALS AND METHODS

Peptide Assembly Modeling

Hyperchem 8.0 was employed to build 3 dimensional renderings of idealized 1:1 Pep2:Heme assemblies. Pep2 was built with an ideal α-helix conformation as supported by our FTIR data. A heme molecule was built as a separate file and merged with the Pep2 file. The heme molecule was placed in an axially coordinating position relative to histidine. The carboxylic acid moieties were placed towards the polar head groups (i.e. K_2E_2) consistent with amphiphilic assemblies. 12 Pep2:Heme molecules were packed to favor bis-histidine coordination as supported by our UV/vis data. CHARMM force fields were employed during energy minimization (*in vacuo*). The resulting structure assists in visualizing a possible assembly driven by the amphiphilic nature of the peptide design while providing a suitable environment for bis-histidine coordination in an α-helix rich environment.

Peptide Synthesis and Purification

All peptides were synthesized on an AAPPTec Apex 396 Automated Multiple Peptide Synthesizer using standard Fmoc chemistry. All coupling reagent solutions were prepared freshly: 20% Piperidine (Sigma-Aldrich) in dimethylformamide, 400 mM O-(Benzotriazol-1-yl)-N,N,N',N'-tetramethyluronium hexafluorophosphate (HBTU, Chem Impex International, Inc.) in dimethlyformamide, and 800 mM diisopropylethylamine (DIEA, Sigma-Aldrich) in dimethylfromamide. All Fmoc protected amino acids were purchased from Chem Impex International, Inc: Fmoc-Lys(Boc)-OH, Fmoc-Glu(OtBu)-OH, Fmoc-Leu-OH, Fmoc-His(trt)-OH. Stock solutions of each peptide were prepared, 4 mM in dimethylformamide. All peptides were synthesized on Rink amide-MBHA resin (0.3 - 0.6 mmol/g, 100 - 200 mesh, Chem Impex International, Inc.).

Resin (0.033 mmol) was loaded in each well of the peptide synthesizer. The peptide was swelled in dimethylformamide for 20 minutes. Deprotection was accomplished by introducing 1.5 mL of the piperidine solution to each well followed by 5 minutes of shaking. A second aliquot of piperidine (1.5 mL) was added to each well followed by 20 minutes of shaking. The resin was washed thrice with fresh DMF. The first amino acid was double-coupled for a total of 120 minutes. Each subsequent amino acid was coupled for 60 minutes. Each coupling introduced 0.50 mL of the amino acid solution followed by 0.50 mL

of the HBTU coupling reagent, followed by 0.50 mL of the DIEA solution. After the final coupling, the deprotection step was utilized to remove the Fmoc N-terminal protecting group and each reaction well was washed three times with dimethylformamide.

Prior to removing the peptide from the resin, each resin was washed with dichloromethane (0.50 mL, 3x) and dried via nitrogen purge (15min). The reaction block was removed from the instrument and added to the cleavage block where vials are positioned below each reaction well. A solution (1.0 mL) of trifluoracetic acid (TFA, 95%), triisopropylsilane (2.5%), and water (2.5%) was added to each reaction well to cleave the peptide from the resin. Total cleavage time was 3 hrs with shaking. The TFA solutions were then passed through the fritted reaction vessels into the collection vials. Each solution was then glass pipetted into 10 mL of cold diethyl ether in a 15 mL Falcon tube. The precipitated peptide was centrifuged for 1 minute and 1000 g using a swinging bucket rotor on a benchtop centrifuge. The pelleted peptide was washed three times by dispersing the pellet in 5 mL of fresh diethyl ether followed by centrifugation (1 min, 1000g).

The peptide was purified via semi-preparative, reversed phase high performance liquid chromatography (RP-HPLC, Agilent 1260 with an autosampler (900 mL injection loop), multiwavelength detector, and autofraction collector). A linear gradient of 4%/min was employed at a flow rate of 2.5 mL/min over 25 minutes from 100% water (Millipore 18.2 MΩ, + 0.1% TFA) to 100% acetonitrile (Sigma-Aldrich, HPLC Grade, + 0.1% TFA). A Phenomenex Jupiter Proteo c-18 column (10 x 250 mm) was used for peptide separation. UV signals were monitored at 220 nm and 280nm. The collected fractions of each peptide were combined and freeze dried (Labconco, Freezone 1.0L). Peptides were verified with electrospray ionization mass spectrometry (Advion, Expression CMS), Figure S1.

Note: TFA removal is essential to facilitate reliable infrared data. Each peptide was resuspended in 30% 10mM hydrochloric acid (HCl) and freeze dried a second time. A minimal or absent peak at 1673 cm^{-1} indicated adequate removal of TFA.

Stock Solutions

Peptides were weighed in a 1.5 mL microcentrifuge tube (2 to 10 mg). Hexafluoroisopropanol was added to each tube to afford a 10 wt% solution. The tube was vortexed until a homogeneous solution was obtained. Next, deuterium oxide (Sigma Aldrich) was added to afford a final 1 wt% solution (pH ~ 4). Heme was weighed in a 1.5 mL microcentrifuge tube (4 to 6 mg). Dimethylsulfoxide was added to afford a 10 mM solution.

Secondary Structural Analysis: Fourier transfer infrared spectroscopy (FTIR) was measured on a Thermo Nicolet 6700 FTIR Spectrometer with an analysis range from 4000 to 1100 cm^{-1} defined by the instrument software as the calcium fluoride (CaF_2) window. The spectra represent an average of 16 scans at 4 cm^{-1} resolution. A demountable solution cell (Sigma Aldrich) using a 0.05 mm Teflon spacer between two CaF_2 windows (32 mm) was employed. A background spectrum of deuterium oxide was measured first. Next, a 1 wt% peptide solution as described in the stock solutions (20 μL) was dropped in the center of one CaF_2 window. With the Teflon spacer in place, the second CaF_2 window was added to the top. The demountable cell was reassembled and introduced to the sample chamber of the FTIR spectrometer. In order to adjust the pH of the sample, 1 μL aliquots of 1 M ND_4OD (deuterated ammonium hydroxide prepared from D_2O and ammonium hydroxide) was added to 100 μL of the 1 wt% stock until a pH of 8 was obtained.

Circular dichroism was employed to corroborate the FTIR data as well as investigate samples at lower concentrations. A Jasco, Inc. J-815 CD spectrometer was employed. Samples (300 μL) were diluted to 250 μM from the 1 wt% stock solutions in either water at pH 4, water at pH 8 (samples adjusted with 1 M NH_4OH), or Tris buffer (50 mM Tris, 100 mM NaCl, pH 8). The samples were placed in a 1 mm pathlength quartz cuvette (Starna Cells Inc.). Each sample was scanned from 260-190 nm with a 0.1 nm data pitch and a 100 nm/min scan rate. Each spectrum represents an average of 3 scans.

The CD data at pH 4 and pH 8 was used to determine the secondary structure distribution. The "Single Spectrum Analysis" on-line tool on the BeStSel website (https://bestsel.elte.hu/index.php) developed by Micsonai et al. was employed for this effort.[21-23] The output file yields a distribution of the following secondary structure features: helix, parallel [beta-sheet], anti-parallel [beta-sheet], turn, and other. We

simplified the output file to highlight only the α-helix and β-sheet (combined parallel and antiparallel) distribution.

Heme Binding and Carbon Monoxide Addition: In order to assess heme binding and subsequent CO addition, samples were prepared inside of a nitrogen purge box (Plas Labs Inc.) and in a custom 2 mm pathlength quartz cuvette equipped with a 14/20 mm female glass joint fitted with a rubber septum. A typical analysis occurs as follows. A diluted stock solution of heme was prepared (25 μM in Tris buffer, pH 8) from the 10 mM Heme stock solution in DMSO described earlier. The solution (900 μL) was transferred to the cuvette. 10 equivalents of peptide (250 μM) was added to the solution. Color changes and aggregation can be noted at this point and vary with each peptide. Sodium dithionite (4.5 μL, 100 mM) was added to the solution and mixed (500 μM final concentration). Typically, the solution changes to a red-orange color indicating successful reduction of the heme from the ferric to ferrous state. Carbon monoxide (Airgas) was delivered via a regulated cylinder equipped with flexible tubing and luer lock needle adapter equipped with a needle. The head space of the cuvette was purged three times for one minute by piercing the septum with the CO delivery needle and vented with a second larger gauge needle. After each CO purge, the solution in the cuvette was mixed via shaking.

UV/vis spectra (Cary 50, 300 to 800 nm, 1 nm data pitch) were recorded after each step to follow the heme spectral changes in response to the addition of the peptide, the reduction via sodium dithionite, and the addition of carbon monoxide.

The fidelity of heme binding was performed by preparing 10 samples with increasing concentrations of peptide. A stock solution of heme 50 μM in Tris buffer, pH 8 was made from the 10 mM Heme stock solution in DMSO. 300 μL aliquots of the 50 μM heme stock solution were placed in 10 microcentrifuge tubes. Varying amounts of peptide yielding final concentrations of 0 to 500 μM were added to the solutions yielding a variation of 0:1 to 10:1 Peptide: heme ratio. UV/visible spectra were collected for all 10 samples

in a 2mm quartz cuvette.The maximum absorption in the Soret was plotted as a function of Peptide:heme ratio. The dissociation constant was then determined by fitting the data to the following equation:

$$y = A0 + (\varepsilon \times l \times 0.5) \times ((\frac{x \times M}{n} + K_D + M) - \sqrt{(\frac{x \times M}{n} + K_D + M)^2 - (\frac{4 \times x \times M^2}{n})} \qquad \text{eq. 1}$$

Where *A0* is the absorption value extrapolated when $x = 0$, ε is the extinction coefficient, *l* is the cuvette pathlength (0.2 cm), *M* is the concentration, *n* is the stoichiometric value (fixed to 1 here), K_D is the dissociation constant, *y* is the absorption, and *x* is the ratio of peptide to heme.

Atomic Force Microscopy: Samples were prepared by first diluting the peptides to 100 μM solutions in either water or water adjusted to pH 8 via 1 M ammonium hydroxide addition. The samples were drop cast onto freshly cleaved mica. The samples interfaced with the mica for 1 minute followed by removal of the solution via pipetting and wicking away excess solution away with filter paper. The sample was then dried for a minimum of 30 minutes. Tris buffer was avoided due to salt contamination upon drying. The samples were imaged with a Multimode 8 Scanning Probe Microscope (Bruker) using Scanasyst cantilevers as well as utilizing the Scanasyst mode (i.e. automated setting of the amplitude setpoint and gain). 2 mm x 2 mm micrographs were obtained at a scan rate of 1 Hz with each line representing 512 data points.

CryoTEM: Sample vitrification for cryoTEM was performed using a Mark IV Vitrobot (ThermoFisher Scientific) Plunge Freezing system for TEM grid preparation. Samples were prepared at 0.2 to 1.0 wt% concentration. 3 μL of the solution was deposited on an ultrathin carbon film on a lacey carbon support, 400 mesh, copper grid (Ted Pella). The sample was imaged by using a Fischione Cryo Transfer Tomography Holder on an FEI-Talos operated at 200kV .

CO Recombination - Transient Absorption Spectroscopy: The same samples described for UV visible spectroscopic characterization (Heme, 25 μM; Peptide, 250 μM; Sodium Dithionite, 500 μM; CO, 980 μM) were used to investigate the CO recombination events facilitated by transient absorption spectroscopy (enVision, Magnitude Instruments). The samples were excited with 355 nm pulsed light (1 ns FWHM) at

100 Hz repetition rate (1 flash every 10 ms) and probed from 400 to 600 nm (5nm steps). The time window for each wavelength was 2.09 ms collecting data at 14 ns/point.

The three dimensional data was transferred to Origin software where the data was reduced by averaging every 20 data points. This effectively reduces the signal to noise.

The heme/CO recombination without peptide was fit to a first order, single exponential process with the following equation:

$$y = Ai \times e^{-kx} + Af \qquad \text{eq.2}$$

Where *Ai*, initial absorbance, *k* is the first order rate constant, *Af* is the final absorption, *y* is the absorption values and *x* is time.

All other data were fit to competitive first and second order rates with the following equation:

$$y = A1 \times e^{-k1x} + \frac{A2}{A2 \times k2 \times x + 1} + Af \qquad \text{eq. 3}$$

Where *A1*, initial absorbance of the first order process, *k1* is the first order rate constant, *A2* is the initial absorbance of the second order process, *k2* is the first order rate constant, *Af* is the final absorption, *y* is the absorption values, and *x* is time.

An average of k_1 and k_2 was determined from six wavelengths, three in the Soret region (400 – 450 nm) and three in the Q-band region (500 – 600 nm). These values were fixed in the analysis of each wavelength in order to (1) reconstruct the 3D data to highlight the efficacy of our analysis and (2) to extract the species associated spectra (SAS) of the first and second order processes. The resulting second order rate constant from the raw data is in units of $Abs^{-1}\ s^{-1}$. The data was converted to $\mu M^{-1}\ s^{-1}$ by changing the ΔmOD y-axis data to Δ[Heme] by utilizing the calculated difference extinction coefficient (Δε) from the steady state data and the cuvette pathlength, 0.2 cm and the data was fit to eq. 3.

RESULTS AND DISCUSSION

Peptide Design: In order to design a peptide capable of helical assembly, cues from *de novo* design strategies combined with the use of repeating amino acids often employed by the peptide materials community are used. Secondary structure propensity tables derived from statistical analysis addressing the frequency at which specific amino acids occur in a given secondary structure, i.e. α-helix or β-sheet, assisted in the determination of which amino acids to choose.[24] While the tables are useful in protein design, the guidance does not always translate well to peptide materials or shorter peptide sequences. For example, an earlier attempt at creating α-helix rich assemblies utilizing the amino acid with highest helix propensity, alanine, yielded β-sheet rich peptides with the sequence K_3A_{12}. Knowing that leucine zippers represent a common motif in α-helix peptide design, we next characterized K_3L_{12} and found a helix rich assembly that could transform into a β-sheet rich assembly upon increasing the temperature or the pH.[25] The leucine rich amphiphilic design is further supported by reports on the peptide R_3L_{12} in which α-helix rich, large hollow tubes are reported at low pH.[19] Here we modified the design to have an electrostatically balanced "cap" (equal number of positively charged lysine (K) and negatively charged glutamic acid (E)) with the sequence H_2N-$K_2E_2L_{12}$-$CONH_2$ (Pep 1), Figure 1. These charged pairs have the potential to form electrostatic interactions within the supramolecular assembly, Figure 2. Leucine also represents a good neighboring amino acid to heme binding sites providing the highest binding affinity when compared to "smaller" amino acids like alanine.[26] Therefore, a heme binding site is engineered into the peptide sequence by placing two histidines in the middle of the poly-leucine block, H_2N-$K_2E_2L_5H_2L_5$-$CONH_2$ (Pep 2). The histidine positioning is intentional as it requires two peptides to bind a single heme molecule resulting in the potential to produce extended networks of heme molecules in a supramolecular arrangement, Figure 2. Finally, the sequences H_2N-$K_2L_{12}E_2$-$CONH_2$ (Pep 3) and H_2N-$K_2L_5H_2L_5E_2$-$CONH_2$ (Pep 4) were designed to probe the positioning of the electrostatic interactions of the peptides when placed at the termini of the peptide. The peptides were synthesized in house following standard Fmoc based solid phase peptide synthesis strategies

and the purity analyzed by reversed phase liquid chromatography with the sequence confirmed by electrospray ionization mass spectrometry.

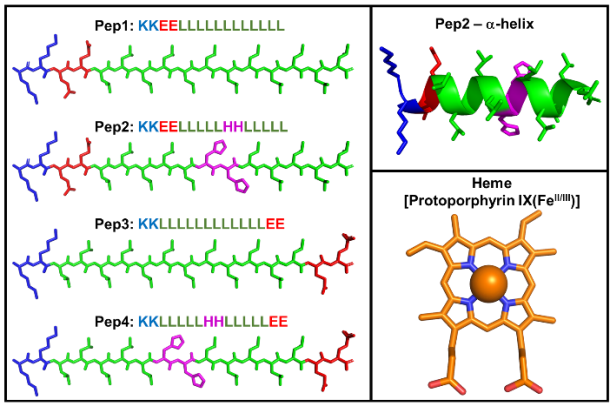

Figure 1. Renderings of Pep1-4 (Color code: Blue, lysine; Red, glutamic acid; green, leucine; purple, histidine), Side view of Pep2 in an a-helix configuration, heme (carbons emphasized in orange).

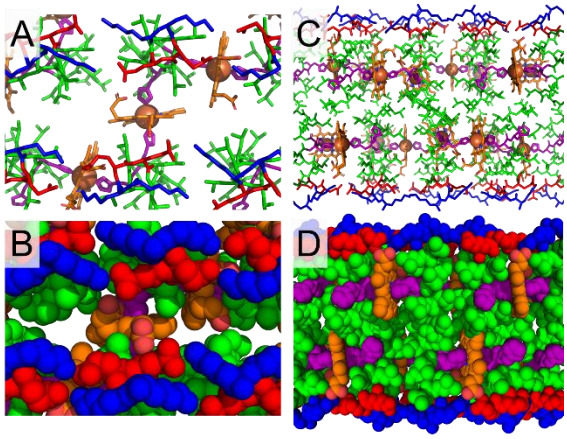

Figure 2. Renderings of an energy minimized structure *in vacuo* of a 1:1 Pep2:Heme assembly when the peptide is in an α-helical conformation. A. top view/stick rendering highlighting the intended bis-histidine coordination of heme, B. top view/space fill rendering highlighting potential electrostatic interactions between positively charged lysine (blue) and negatively charged glutamic acid (red), C. side view/stick rendering, and D. side view/space fill rendering highlighting the proposed amphiphilic assembly with the hydrophobic poly-leucine interior emphasized in green. (Color code: Blue, lysine; Red, glutamic acid; green, leucine; purple, histidine),

Peptide Solubility: Pep 1 and Pep 3 have poor solubility due to their highly hydrophobic poly-leucine sequence. Therefore, the samples were prepared first at 10wt% in hexafluoroisopropanol (HFIP) and then diluted to 1wt% in deuterium oxide for infrared spectroscopy investigations. While Pep2 and Pep4 are soluble in water, attributed to the two hydrophilic histidines in the core of the leucine sequence, the stock solutions were prepared similarly to that for Pep1 and Pep 3. Over the course of 2 days, Pep 1 and Pep 2 remained as free flowing solutions, while Pep 4 had an increase in viscosity. Pep 3 resulted in a self-supporting hydrogel. Peptide solutions for spectroscopic characterization were then prepared in Tris Buffer (50 mM Tris, 100 mM NaCl, pH 8.0). pH 8 was used to ensure the deprotonation of the imidazole nitrogen on histidine to enable heme binding.

Peptide Secondary Structure: The peptide stock solutions were prepared in D_2O in order to perform infrared (IR) spectroscopy ([Pep] = 1wt% 5.2 mM).[27] The data are summarized in Table 1. Dilute solutions were prepared for circular dichroism (CD) studies ([Pep] = 250 μM in water, pH 4 and 8, and Tris Buffer, pH 8) to investigate any structural sensitivity in response to concentration changes. All samples indicated a sensitivity to both pH and buffer, Figure 3-4 and Figures S2-3.

Pep 1 at pH 4 indicated a mixture of β-sheets and α-helices by both IR (Figure S2A, amide 1 vibrations at 1624 cm^{-1} and 1658 cm^{-1})[27-28] and CD (broad spectrum consisting of a mixture of 208, 222 and 218 features, Figure 4A).[29] Upon increasing the pH to 8 we observe a similar distribution by the infrared spectra, however, the CD spectra indicate a loss in signal intensity which is often an indicator of aggregation, Figures 3A and 4A. Upon preparation in Tris buffer, the peptides yield aggregate structures with low intensity signals, Figure S3A. The IR spectra suggest again a mixture of α-helices and β-sheets.

Pep 2 indicated a high percentage of α-helix conformation by both CD (Figure 4B, minima at 208 and 222) and IR spectroscopy (Figure 3B, amide I = 1649 cm^{-1}) Furthermore, the ellipticity ratio of 222 nm/208 nm < 1.0, indicating solubilized helices. Upon increasing the pH to 8, maintenance of the helices are observed but evidence of assembly is noted by the change of 222 nm /208 nm > 1.0. This feature is

often associated with assembled α-helices or α-helices in a lipid bilayer environment.[30] IR data supports the maintenance of the α-helix structure with a dominant peak observed at 1653 cm^{-1}. When prepared in Tris buffer at pH 8, similar features are observed but the intensity of the CD spectrum is dramatically decreased due to aggregation. When compared to Pep 1, the introduction of more polar residues like histidine aid in the solubility of the peptide as well as prevent any formation of β-sheets.

Pep 3 yielded β-sheets. This is consistent with other β-sheet rich peptide assemblies that yield self-supporting hydrogels at low weight percentage. The IR indicated a clear β-sheet assembly with amide I vibrations of 1626 cm^{-1} and 1690 cm^{-1} (Figure 3C) while the CD spectra indicated a minima at 218 nm, Figure 4c.[27-29] Similar results were obtained at pH 8. Preparation of the sample in Tris buffer indicated a dramatic loss in CD signal intensity most likely due to aggregation, Figure 4C. The IR data, however, confirmed the maintenance of β-sheets, Figure S3C.

Pep 4 was similar to Pep 1 in that it yielded a mixture of α-helices and β-sheets, Figure 3D. The pH sensitivity was greater than Pep 1 and Pep 3 owing to the two histidines in the center of the hydrophobic region. Not only does this feature enhance the solubility of the peptide, but also promotes a small population of the assemblies to yield α-helix structures. Upon increasing the pH above the pKa of histidine as well as in Tris buffer pH 8, the peptide assembles into visible aggregates yielding dramatic losses in signal intensity in both IR and CD spectra, Figures 4D, S2D, and 4D.

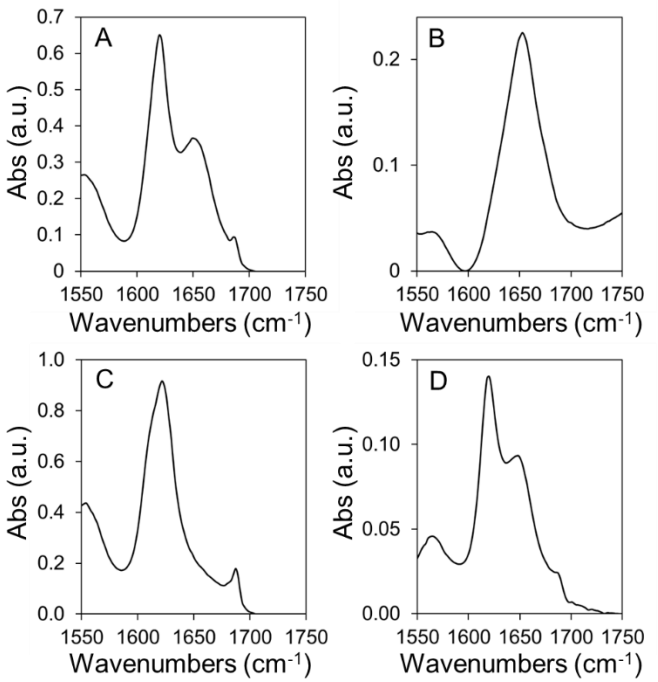

Figure 3. Amide I region of the FTIR spectrum in D_2O at pH 8. A, Pep1; B, Pep2; C, Pep3; and D, Pep4. Additional secondary structure analysis, FTIR at pH 4 and TRIS Buffer at pH 8 is in the supporting online data.

Peptide	Amide I (cm^{-1}) pH 4	Amide I (cm^{-1}) pH 8	Amide I (cm^{-1}) Tris, pH 8
Pep1	1624, 1658	1620, 1649	1622, 1653
Pep2	1649	1653	1651
Pep3	1626	1622	1624
Pep4	1622, 1649	1620, 1649	1626, 1647

Table 1. Amide I vibrations for all peptides.

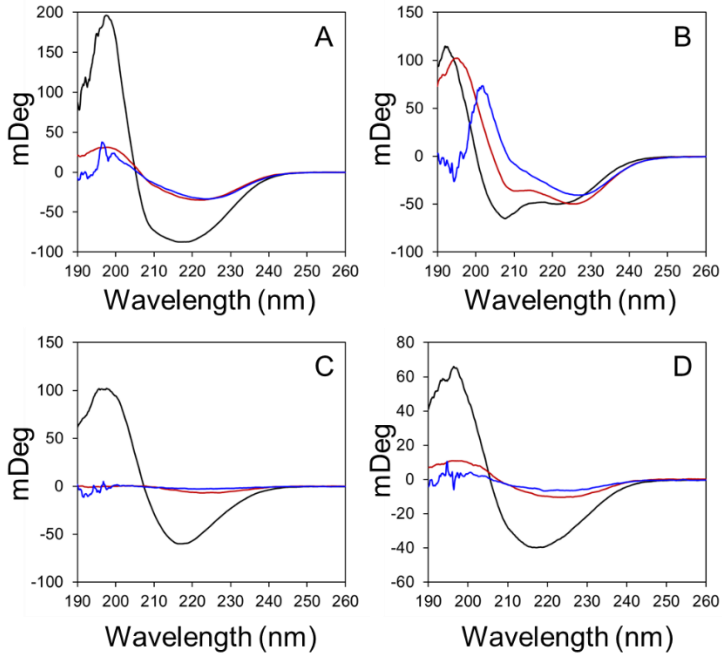

Figure 4. CD spectra of A, Pep1; B, Pep2; C, Pep3; and D, Pep4, at pH4 (black), pH 8 (red), and Tris buffer, pH 8 (blue). [Pep] = 250 μM.

The CD spectra were further analyzed with the on-line tool, BeStSel, for each peptide to yield a distribution of secondary structural features.[21-23] The results are presented in Figure S4. The amphiphilic designs, Pep1 and Pep2 at pH 4 are dominated by an α-helix conformation at 94% and 84% respectively. The bola-amphiphilic designs Pep3 and Pep4 are dominated by a β-sheet conformation at 94% and 68%, Figure S4B. Upon increasing the pH there is a noticeable shift in the distribution with Pep1, 3, and 4 favoring a β-sheet conformation. Pep2 is the only peptide that remains predominantly in the α-helix conformation at 70%. These data are consistent with the interpretation of the FTIR data presented earlier.

All in all, the secondary structure is dramatically responsive to the placement of the histidine residues in the hydrophobic core impacting not only the solubility but the distribution of assembly. The histidines create a pH responsiveness that triggers self-assembly similar to what we identified in our heme binding, β-sheet rich peptide amphiphile studies.[31] Furthermore, when the electrostatic pairs of glutamic

acid (E) and lysine (K) are placed on either end of the leucine block in a bola-amphiphilic design (e.g. Pep3 and Pep4), β-sheet conformations are more likely to be promoted than α-helices. Pep 2 facilitates the investigation of heme binding and functional properties in an α-helix rich, self-assembled environment, unique from previously reported heme binding peptide assemblies.

Material Morphology: Atomic force microscopy reveals the morphology of the materials. Images were obtained of the samples drop cast from 100 μM samples at both pH 4 and 8, Figure 5. The samples at pH 8 include heme to highlight that heme has little to no influence over the final assembly. We avoided samples prepared in Tris buffer as efficient removal of the salt proved challenging. CryoTEM was obtained for Pep1-4 at pH 4 to ensure that the structures observed by AFM were not influenced by the interface of the peptide with the mica surface, Figure S5. All CryoTEM images are consistent with the AFM data.

Pep1, which yielded a mixture of α-helices and β-sheets, yields two distinct features, discs and fibers, Figure 5a. The sequence, $K_2E_2L_{12}$, is very similar to a previously reported peptide K_3L_{12} where similar disks and fibers were observed.[25] In that particular study, morphological change correlated to secondary structure as a response to increasing pH was observed. α-helix rich structures were correlated to the disks and the β-sheet rich structure were correlated to the fibers. Upon increasing the pH to 8 and in the presence of heme, we observe aggregates of fibers, Figure 5e.

The micrographs (AFM and CryoTEM) representing Pep2 at pH 4 indicates few superhelical fibers, Figure 5b. However, the majority of the sample is in the background as small nanometer sized aggregates. Upon increasing the pH to 8 and in the presence of heme, the sample yields small spherical aggregates in a wide range of sizes with a few superhelical fibers, Figure 5f.

Pep3 and Pep4, indicated the formation of fibers at pH 4, Figure 5c-d. This is not surprising for Pep3 as the IR and CD spectra indicate β-sheet rich assemblies which strongly correlate to fibril morphologies. Upon increasing the pH to 8, the fibers were noted to aggregate for both Pep3 and Pep4.

The microscopy reveals a conundrum in our design process as well distributed nanoscale features are observed at pH 4. In general, increasing the pH to 8, above the pKa of histidine, the nanoscale assemblies aggregate. However, the deprotonation of histidine is essential for successful heme coordination in these assemblies. In future iterations, careful curation of the electrostatic interactions must be considered to ensure both well-dispersed nanoscale materials and heme binding.

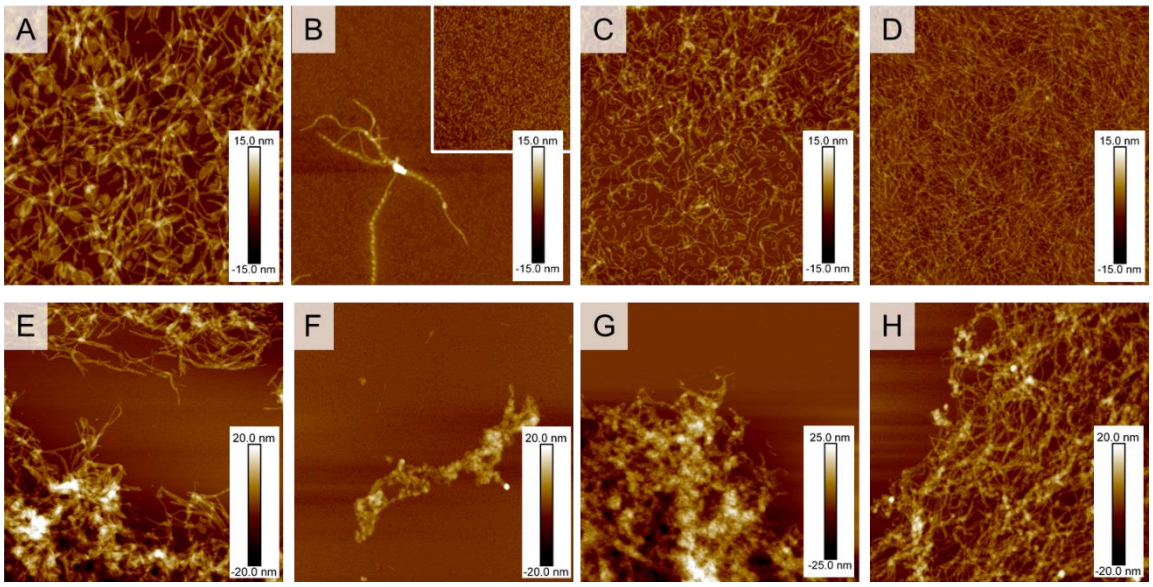

Figure 5. Atomic force micrographs (2 μm x 2 μm) of peptide assemblies deposited from solutions at pH 4: A. Pep1, B. Pep2, C. Pep3, and D. Pep 4 and deposited from solutions at pH 8 containing heme: E. Pep1, F. Pep2, G. Pep3, and H. Pep 4. The scale bars (inset) represent the height. The inset of **Figure** B represents an enhanced contrast to highlight the presence of small assemblies in the background.

Heme binding and Function (CO Binding): In order to investigate heme binding to the peptide assemblies as well as reduction to ferrous heme and carbon monoxide adduct formation, Pep 1-4 (250 μM final concentration) were added to Heme in tris buffer (25 μM in Tris buffer, pH8) reduced with sodium dithioionite (500 μM) followed by addition of carbon monoxide. The changes in the electronic absorption spectra were noted and summarized in Table 2 and are representative of heme proteins and peptides reported

in the literature.[14] In order to assess the fidelity of heme binding to each assembly, dissociation constants were determined (Table 2) by performing a careful titration for each peptide where the concentration was varied from 1 to 10 equivalents of peptide while observing changes in the spectrum, Figure S7 and analyzed for K_D using equation 1.

In the absence of peptide, heme free in solution yields a spectra with Soret maximum at 383 nm and Q-bands at 500 and 620 nm, **Figure** S6. Upon reduction, a slight shift to 379 nm (409 nm shoulder) and a broad peak at 560 nm are observed. In both the ferric and ferrous states, the blue shifted, broad spectra indicate that the heme molecule aggregates in Tris buffer.[32] However, upon addition of CO, a notable shift and sharpening of the Soret band is observed, Soret, 406 nm; Q-band 532 and 563 nm. Similar data has been reported for CO bound to heme monomers in CTAB micelles.[33] This indicates that CO coordination is sufficient to break up heme aggregates even in the absence of a protein or peptide assembly.

The addition of Pep 1 to a heme solution yielded a shift in the Soret maximum to 406 nm, Figure 6A. This is similar to a heme molecule being solubilized in a hydrophobic environment without axial coordination by histidine as none are available.[34-35] Pep 3 + heme yields a broad spectrum similar to that of heme free in solution. However, it has been noted that upon centrifugation, the heme pellets with the peptide assembly thus indicating that it is integrated into the assembly, but not in a discrete, hydrophobic binding environment. Upon adding Pep2 or Pep4 to the heme solution, the color visibly changes from green to orange/red yielding peaks at 412 and 532 (560 shoulder) nm. The spectra representing Pep2 and Pep4 plus heme are consistent with bis-histidine axial ligation to the ferric center of the heme molecule.[14] Interestingly, the titration data yielding the dissociation constants (eq. 1) indicate that Pep2 binds heme with nearly one order of magnitude greater affinity ($K_D = 5.1 \times 10^{-5}$ M) when compared to Pep4 ($K_D = 41 \times 10^{-5}$ M), Figure S7. This can potentially be correlated to the α-helix conformation of the Pep2 assembly yielding a more favorable binding site. Not surprisingly the dissociation constants for Pep1 ($K_D = 89 \times 10^{-5}$ M) is higher because the assembly does not offer a histidine binding site and the heme molecules are simply embedded in the hydrophobic pocket of the assembly. Pep3 had some observable spectral changes, i.e. a

decrease in absorption followed by a slight increase indicating a possible association to the assembly, but the data were not suitable for analysis and therefore the K_D value was not quantified.

Since Pep2 and Pep4 were determined to bind heme via histidyl coordination, it was not surprising to see the resulting canonical ferrous (Fe^{2+}) heme spectra, Soret, 424 nm; Q-bands, 527, 558 nm. Since Pep1 does not offer a histidine for axial coordination yet still breaks up heme aggregates in a hydrophobic environment, it was not surprising to note a slightly blue shifted spectrum (Soret, 421 nm; Q-bands, 526, 557 nm. Finally, reduction of heme in the presence of Pep3 looked similar to that of reduced heme in buffer suggesting that heme remains outside of the self-assembled structured. The data for Figure 6 is summarized in Table 2.

The event of heme binding CO has relevance in biosensing as well as implications in catalytic function as it addresses the accessibility of the heme active site by a small molecule.[36-37] CO was found to bind to all heme peptide assemblies investigated with similar spectral features, Figure 6 and Table 2. It is important to note that the addition of CO breaks up the heme aggregates. When compared to the free Heme-CO complex there is a 12-13 nm red shift in the Soret region when Pep1-4 is introduced. We propose that the heme-CO complex is embedded in the hydrophobic core of all structures at this point.

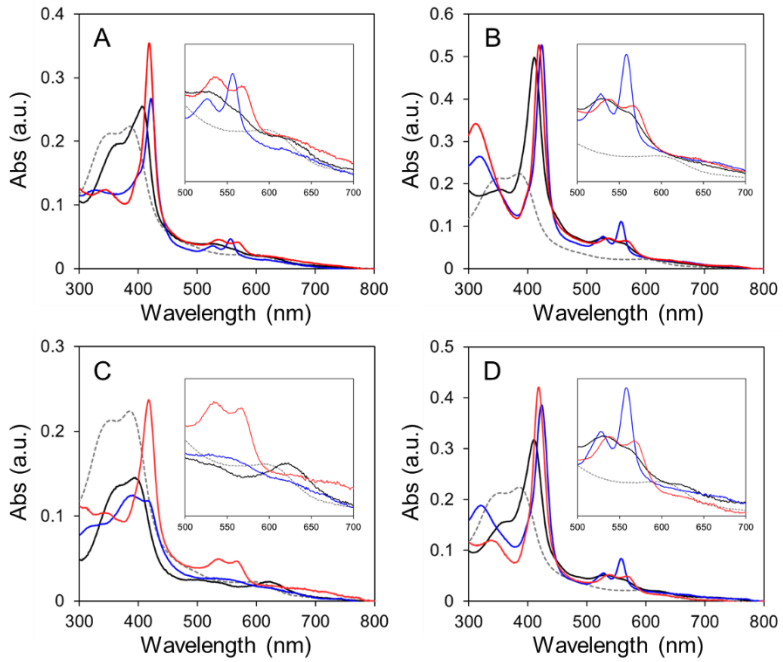

Figure 6. Electronic absorption spectra of A, Pep1; B, Pep2; C, Pep3; and D, Pep4. [Heme] = 25 μM, [Pep] = 250 μM in Tris buffer, pH 8. Free heme (dashed line), Heme + Peptide (black line), Reduced (blue line), carbon monoxide bound (red line). See supporting online information for Free Heme-CO Spectra.

Peptide	Peak	Ferric (Fe^{3+})	Ferrous (Fe^{2+})	CO-Adduct	K_D (M)
None	Soret	383	379, 409 (sh)	406	NA
	Q-Band	593	560 (br)	532, 563	
Pep1	Soret	406	421	418	89×10^{-5}
	Q-Band	520, 620 (sh)	526, 557	536, 567	
Pep2	Soret	412	424	419	5.1×10^{-5}
	Q-band	531, 560 (sh)	528, 558	536, 565	
Pep3	Soret	394	391, 414	417	NB*
	Q-band	621	550, 650	537, 567	
Pep4	Soret	410	423	418	41×10^{-5}
	Q-band	531, 560 (sh)	528, 558	538, 567	

Table 2. Summarized UV/visible spectroscopic data of heme binding, reduction, and CO binding to Pep1-4. Dissociation constants are representative of ferric (Fe^{3+}) heme binding to each peptide assembly in Tris buffer at pH 8. *NB: no binding determined.

Carbon Monoxide Binding Dynamics: In order to highlight the ability of our materials to function like heme proteins, a series of experiments highlighting the binding of CO and photoinitiated release of CO and subsequent recombination have been measured. The ability to bind CO to the heme active site highlights

the chromophore's ability to bind small molecules in a similar fashion to heme proteins thus supporting its potential role in catalytic processes like CO_2 conversion.

Photodissociation of CO from the heme active site is a method that historically has been used to probe the dynamics of heme binding pockets.[36-39] Typically, CO recombination with heme occurs within microseconds. Variations in the rate of CO recombination facilitate the interpretation of whether the heme binding site is perturbed due to amino acid axial ligation or unperturbed due to an open heme site. In addition, the rigid environment of a peptide assembly when compared to a more dynamic structure like a globule heme protein may influence the rate of CO recombination. Transient absorption spectroscopy captures this process and the results are summarized in Table 3.

First, heme + CO recombination was measured in the absence of peptide, [Heme] = 25 μM + $[CO]_{sat}$ = 980 μM. Upon excitation with 355 nm light, an immediate bleach of the Soret band representing the heme-CO adduct is observed, Figure S8 and S9. Interestingly, a transient species at 420 nm is observed that is not apparent in the calculated difference spectrum [Heme(reduced) – Heme(CO)], Figure S10. In the steady state UV-visible spectrum, the data of Heme(reduced) is representative of an aggregated state as the planar, hydrophobic molecules indicates a blue-shifted and broad peak at 379 nm. In addition, the Q-band region highlights two bleached transitions at 530 and 560 nm consistent with the calculate difference spectrum. The transient signal, therefore, represents heme in the monomeric, non-aggregated, reduced state. The data fit to a single exponential decay, Figure S9 and equation 1. Typically, heme-CO recombination follows pseudo-first order kinetics due to the fact that the system is saturated with the binding analyte.[39] CO is in 40 fold excess in this case (980μM/25 μM) and therefore is consistent with literature reports. The observed rate constant was determined to be 5.1×10^4 s^{-1}.

In the presence of the peptide assemblies, Pep 1-4, the kinetics were more complicated. The samples measured were [Heme] = 25 μM, [Pep] = 250 μM, and $[CO]_{sat}$ = 980 μM in Tris buffer pH 8. Interestinglythe transient species were similar in all cases Figures 7, 8, S11-19, but the rate constants varied

depending on the presence of heme-coordinating amino acid, histidine, Table 3. Upon excitation with 355 nm light, an immediate bleach of the Soret band representing the heme-CO adduct is observed while a transient species observed at 435 nm is representative of the reduced heme species, Figure 7. In spite of the pseudo-first order conditions, the kinetics follow a fast first order process combined with a slower second order CO recombination process, Figure 8. However, the peptides investigated here are not typical globular heme proteins that follow pseudo-first order CO recombination. The self-assembled peptide materials yield large aggregates of either spherical or fibril-like assemblies. In order for CO recombination to follow pseudo-first order recombination kinetics, the CO must diffuse away from the heme-site and peptide assembly and the excess CO can recombine. We propose that upon CO dissociation, the free CO is embedded in the peptide material and does not diffuse in the assembled peptide environment resulting in an apparent second order A + B → C reaction as opposed to the typical pseudo-first order, A + xs B → C.

Figure 7 highlights the experimental results and the fitted spectral changes over 2 ms of CO recombining to the α-helix rich Pep2:Heme assembly ([Peptide]:[Heme] = 10:1). The data was fit to a fast first order process (k_1) and a slower second order process (k_2) Figure 8 and equation 3. The two component process is highlighted by the wavelength dependent kinetics. The kinetics at 435 nm follows the recovery of transient species while the kinetics at 560 nm indicates an initial bleach followed by the formation of a transient species that recovers to baseline at times longer than 2 ms, Figure 8. The species associated spectra (SAS) were extracted to highlight the difference spectra associated with the first order process (SAS1) and the second order process (SAS2). SAS2 (Figure 8 C&D) clearly resembles the calculated difference spectra of Pep2:Heme (reduced) – Pep2:Heme-CO, Figure S13. The Q-band region of SAS1 (Figure 8D) indicates a bleach of the CO-adduct at 538 and 560 nm. Furthermore, the observed first order rate constant (k_1) in each Pep:Heme assembly is ~ 10^4 s^{-1} similar to what was characterized for free heme under these conditions. Therefore, we propose that SAS1 represents a contribution from CO-dissociating from free heme.

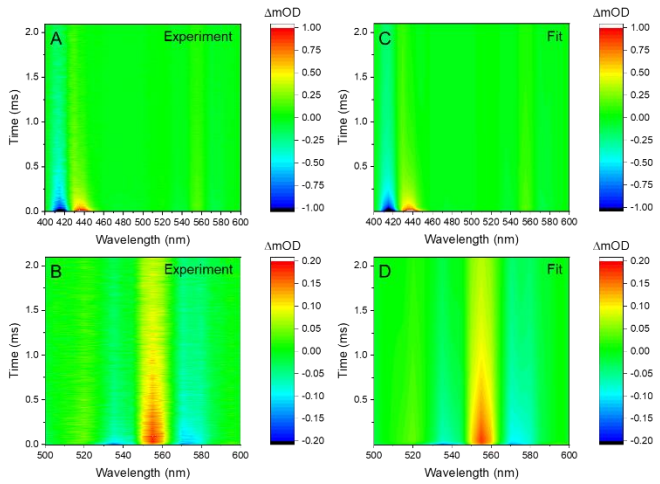

Figure 7. Transient absorption spectroscopy of CO recombination to Pep2:Heme assembly in Tris Buffer, pH 8. A is the experimental data from the full spectrum and B is the experimental data from the Soret region. C and D represent the fitted data of the first order + second order recombination rates.

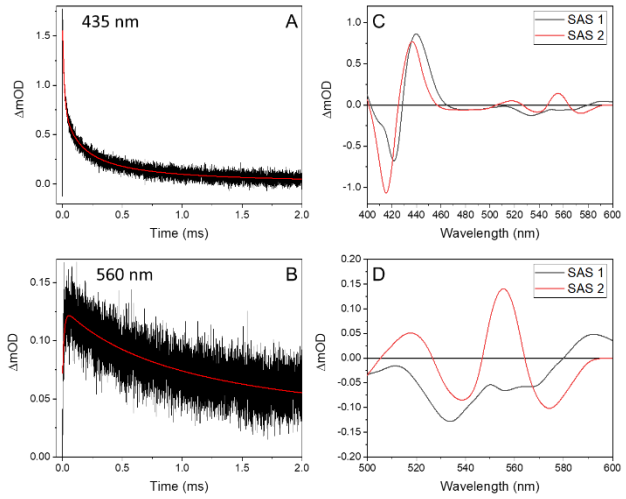

Figure 8. Kinetics of Pep2:Heme CO recombination monitored at A. 435 nm and B. 560 nm. The red line represents the kinetic fit, fast first order followed by a slow second order process. Species associated spectra (SAS) of C. the full spectrum, and D. The Q-band region where SAS1 represents the first order data and SAS2 represents the second order data.

Interestingly, despite not possessing a histidine rich, heme coordination environment, CO recombination to Pep1:Heme indicated similar behavior of a fast first order process followed by a slower second order process, Figure S11-12. However, the determined second order rate constant was one order of magnitude greater than that found for Pep 2:Heme, Table 3. Pep4:Heme was also investigated (Figure S18-19) and yielded very similar first and second order rate constants as those described for Pep2:Heme-CO. Pep 3:Heme-CO recombination did not follow clean CO recombination kinetics. In Figure S14-17, the data were fit to the same first + second order rates but a global fit was never realized as either the Soret region (Figures S14-15) or the Q-band region (Figures S16-17) were poor fits to the model. The steady state spectra suggest that the heme was not embedded in a hydrophobic pocket prior to CO binding. Therefore, it is possible that heme is free in solution, embedded in the self-assembly matrix, and/or buried in the hydrophobic pocket thus complicating the CO recombination analysis. In our analysis, k_2 was determined to be nearly two orders of magnitude greater (i.e. fasted) than that for Pep2 and Pep4, Heme CO recombination.

Table 3. Summary of the kinetics of CO recombination where k_1 represents the pseudo-first order recombination of CO of free heme either in solution or embedded in the peptide assembly matrix, k_2 represents the raw second order rate constant averaged over multiple wavelengths and the third column k_2* represents the second order rate in $\mu M^{-1}\ s^{-1}$ determined from a single wavelength.

Peptide	k_1 (s^{-1})	k_2 ($Abs^{-1}\ s^{-1}$)	k_2* ($\mu M^{-1}\ s^{-1}$)
None	$5.1 \pm 0.7 \times 10^4$	NA	NA
Pep1	$7.3 \pm 2.9 \times 10^4$	$33 \pm 13 \times 10^{-3}$	$27 \pm 20 \times 10^4$
Pep2	$6.6 \pm 0.6 \times 10^4$	$7.0 \pm 2.0 \times 10^{-3}$	$4.1 \pm 0.5 \times 10^4$
Pep3	$5.8 \pm 3.9 \times 10^4$	$180 \pm 70 \times 10^{-3}$	$140 \pm 40 \times 10^4$
Pep4	$5.3 \pm 0.4 \times 10^4$	$6.8 \pm 0.8 \times 10^{-3}$	$3.5 \pm 0.9 \times 10^4$

From these results some general observations can be made. The coordination environment or the lack thereof has a direct impact on the CO recombination kinetics. Pep2 and Pep4 coordinate heme via histidine to the iron center which inhibit CO recombination as opposed to Pep1 and Pep3 that simply offer a hydrophobic environment for heme. As a result, CO recombination to Pep2 and Pep4 is slower than the unencumbered Pep1 and Pep3 heme environment. This trend has been previously reported as a result of site directed mutagenesis studies of myoglobin in which a 2 order of magnitude increase in the CO recombination rate constant is reported.[40]

To compare our rate constants to reported literature values, single wavelength kinetics at 435 nm were used to determine the rate constant in $\mu M^{-1}\ s^{-1}$ (k_2*) by converting the ΔmOD value to Δ[Heme] by using the extinction coefficient difference (Δε) determined from the steady state difference spectra, $\Delta\varepsilon_{435nm}$ = 25,000 $M^{-1}\ cm^{-1}$. The results are summarized in Table 3. Our values are nearly 4 to 6 orders of magnitude greater than what has been previously reported for 6 coordinate (i.e. bis-his coordinated) heme proteins,[36] 3 – 90 $\mu M^{-1}\ s^{-1}$ and *de novo* heme proteins,[37] 0.8 – 11 $\mu M^{-1}\ s^{-1}$. Interestingly, in myoglobin CO recombination studies where the distal-histidine is mutated to a non-coordinating aliphatic amino acid, a one to two order of magnitude increase in the rate constant is observed: wild type myoglobin (11.4 $mM^{-1}\ s^{-1}$), H64V (160 $mM^{-1}\ s^{-1}$), and H64L (1100 $mM^{-1}\ s^{-1}$).[40] However, our reported data represent direct second order processes and are not extrapolated values.

When considering the literature values of CO dissociation from Heme proteins, the CO recombination dynamics to Pep 1-4/Heme assemblies are more complicated due to the supramolecular arrangement of heme molecules. In examples of globule proteins, CO can diffuse into solution leading to the pseudo-first order behavior whereas the CO may not diffuse away from peptide assembly matrix in Pep1-4:Heme assemblies leading to an apparent second order rate of recombination. Therefore, we suggest that the slower rates of recombination and the directly measured second order rate constant are due to a rigid environment of the self-assembled structure, when compared to globular heme proteins, and

directly impacts CO diffusion, the dynamics of the hydrophobic interior, and the histidine ligation dynamics with heme.

Design Principles and Room for Improvement: Exploring the impact that α-helices versus β-sheet arrangement has on the overall function and materials properties is of great interest in developing new functional peptide materials. The prevalence of β-sheets in self-assembled peptide materials highlights the need for understanding the design principles of peptide design. *De novo* designed helical bundles are incredibly well understood and offer an intersection between protein and peptide design where design criteria are complementary but not the same.[37, 41-42] This was noted earlier when observing that poly-alanine in short peptides does not promote α-helices in spite of the fact that alanine possesses the highest propensity for occurring in a helical structure. The work by Zhang et al. [18] highlights the ability to develop long range ordering of helices through more sophisticated computational methods. While successful, these design principles stem from the protein data bank, while peptide self-assembly relies on materials that do not crystallize as their supramolecular properties represent an aspect of their material nature that cannot be compromised. Peptide materials design principles, therefore, have a unique set of design criteria that does not always follow the rules of protein design. However, some simple design criteria can be adopted such as the heptad pattern utilized in designing helical bundles. By utilizing the helical wheel diagram, specific interfaces can be generated to control long rang ordering, or perhaps promote fibril formation that does not aggregate yet retains its α-helical secondary structure.

Implications from CO binding: The carbon monoxide binding studies represent an older method that utilizes the redox inactive carbon monoxide molecule as a surrogate to oxygen binding. Interestingly, our results follow second order rate laws while the vast majority of the literature of globule heme proteins report pseudo first order rate processes. We propose that this is due to the trapping of the CO by the peptide assembly matrix making it an interesting tool in the application of heme peptide assemblies where their function falls somewhere between enzymes and catalytic materials. Rate constants obtained here provide significant insight into the binding pocket surrounding the heme molecule. Here, we do not see much of a

difference between the α-helix rich, heme binding peptide assembly of Pep2:Heme and the β-sheet rich, heme binding pocket of Pep4:Heme. However, the morphologies of the two peptide assemblies similarly yield bis-histidine coordination in a leucine rich environment. The absence of histidine coordination yields an unperturbed heme molecule embedded in a hydrophobic environment where the second order rate constant is nearly one order of magnitude greater for Pep 1: Heme and nearly two orders of magnitude greater for Pep 3: Heme. The impact that coordination has on the rate of recombination of CO is consistent with that reported for heme proteins and therefore, the design strategy for controlling the rate of small molecule binding to the active site of the heme peptide materials reported is directly translatable from the heme protein literature. Finally, the natural proteins are often cited as being useful CO or NO biosensors. Heme peptide self-assembled materials, however, offer a synthetic alternative to the naturally occurring systems. It is demonstrated here that simple design strategies can afford tailorable sensing parameters as evidenced by the peptide sequence dependence on CO recombination rates.

CONCLUSIONS

Pep1-4 were synthesized to explore the design strategy of simple peptides that are capable of self-assembling into α-helix rich structures and are capable of coordinating heme. The sequence Pep2 - H_2N-$K_2E_2L_5H_2L_5$-$CONH_2$ employs an electrostatically balanced head group (2 lysine (+) and 2 glutamates (-) and poly-leucine blocks to promote helix formation. As a result, Pep2 is capable of (1) folding into an α-helix, (2) assembling into a spherical structure, (3) coordinating heme, and (4) reversibly binding carbon monoxide. The two histidine residues placed in the middle of the poly-leucine blocks serve as the heme binding site with the potential to bridge one heme molecule between two peptides. Pep-4 H_2N-$K_2L_5H_2L_5E_2$-$CONH_2$ functions similarly to Pep-2 but forms β-sheet rich fibrils. This simple design change of electrostatic residue positioning highlights the sensitivity of short peptide sequences that makes rational design processes challenging. Interestingly, the two peptide heme assemblies, despite their difference in secondary structure, yielded similar rates of CO recombination under the conditions investigated. Our future design efforts will explore optimizing the hydrophobic interface by using helix/heptad inspired patterning

and continued efforts in variations of electrostatic patterning to yield more pristine nanoscale architectures reminiscent of the β-sheet rich assemblies that dominate the peptide materials field.

SUPPORTING INFORMATION: Additional Figures reporting additional infrared spectra, circular dichroism spectra, UV/vis spectra, and transient absorption spectra are available online.

ACKNOWLEDGEMENTS: Work performed at the Center for Nanoscale Materials, a U.S. Department of Energy Office of Science User Facility, was supported by the U.S. DOE, Office of Basic Energy Sciences, under Contract No. DE-AC02-06CH11357.

REFERENCES

1. Levin, A.; Hakala, T. A.; Schnaider, L.; Bernardes, G. J.; Gazit, E.; Knowles, T. P., Biomimetic peptide self-assembly for functional materials. *Nat. Rev. Chem.* **2020,** *4* (11), 615-634.

2. Sato, K.; Hendricks, M. P.; Palmer, L. C.; Stupp, S. I., Peptide supramolecular materials for therapeutics. *Chem. Soc. Rev.* **2018,** *47* (20), 7539-7551.

3. Huo, Y.; Hu, J.; Yin, Y.; Liu, P.; Cai, K.; Ji, W., Self-Assembling Peptide-Based Functional Biomaterials. *ChemBioChem* **2023,** *24* (2), e202200582.

4. Sinha, N. J.; Langenstein, M. G.; Pochan, D. J.; Kloxin, C. J.; Saven, J. G., Peptide design and self-assembly into targeted nanostructure and functional materials. *Chem. Rev.* **2021,** *121* (22), 13915-13935.

5. Mitrovic, J.; Richey, G.; Kim, S.; Guler, M. O., Peptide Hydrogels and Nanostructures Controlling Biological Machinery. *Langmuir* **2023,** *39* (34), 11935-11945.

6. Kim, J.-e.; Kang, J. H.; Kwon, W. H.; Lee, I.; Park, S. J.; Kim, C.-H.; Jeong, W.-j.; Choi, J. S.; Kim, K., Self-assembling biomolecules for biosensor applications. *Biomater. Res.* **2023,** *27* (1), 127.

7. Lee, J.-H.; Lee, J. H.; Lee, Y. J.; Nam, K. T., Protein/peptide based nanomaterials for energy application. *Curr. Opin. Biotechnol.* **2013,** *24* (4), 599-605.

8. Bhaskar, R.; Zo, S. M.; Narayanan, K. B.; Purohit, S. D.; Gupta, M. K.; Han, S. S., Recent development of protein-based biopolymers in food packaging applications: A review. *Polym. Test.* **2023,** *124*, 108097.

9. Hatanaka, T.; Matsugami, A.; Nonaka, T.; Takagi, H.; Hayashi, F.; Tani, T.; Ishida, N., Rationally designed mineralization for selective recovery of the rare earth elements. *Nat. Commun.* **2017,** *8* (1), 15670.

10. Maeda, Y.; Makhlynets, O. V.; Matsui, H.; Korendovych, I. V., Design of catalytic peptides and proteins through rational and combinatorial approaches. *Annu. Rev. Biomed. Eng.* **2016,** *18*, 311-328.

11. Zou, Q.; Liu, K.; Abbas, M.; Yan, X., Peptide-Modulated Self-Assembly of Chromophores toward Biomimetic Light-Harvesting Nanoarchitectonics. *Adv. Mater.* **2016,** *28* (6), 1031-1043.

12. Reedy, C. J.; Gibney, B. R., Heme Protein Assemblies. *Chem. Rev.* **2004,** *104* (2), 617-650.

13. Ing, N. L.; El-Naggar, M. Y.; Hochbaum, A. I., Going the Distance: Long-Range Conductivity in Protein and Peptide Bioelectronic Materials. *J. Phys. Chem. B.* **2018,** *122* (46), 10403-10423.

14. Lombardi, A.; Nastri, F.; Pavone, V., Peptide-based heme− protein models. *Chem. Rev.* **2001,** *101* (10), 3165-3190.

15. Solomon, L. A.; Kronenberg, J. B.; Fry, H. C., Control of Heme Coordination and Catalytic Activity by Conformational Changes in Peptide–Amphiphile Assemblies. *J. Am. Chem. Soc.* **2017,** *139* (25), 8497-8507.

16. Fry, H. C.; Wood, A. R.; Solomon, L. A., Supramolecular control of heme binding and electronic states in multi-heme peptide assemblies. *Org. Biomol. Chem.* **2017,** *15* (32), 6725-6730.

17. Fry, H. C.; Divan, R.; Liu, Y., Designing 1D multiheme peptide amphiphile assemblies reminiscent of natural systems. *Nanoscale.* **2022,** *14* (28), 10082-10090.

18. Zhang, H. V.; Polzer, F.; Haider, M. J.; Tian, Y.; Villegas, J. A.; Kiick, K. L.; Pochan, D. J.; Saven, J. G., Computationally designed peptides for self-assembly of nanostructured lattices. *Sci. Adv.* **2016,** *2* (9), e1600307.

19. Castelletto, V.; Seitsonen, J.; Ruokolainen, J.; Piras, C.; Cramer, R.; Edwards-Gayle, C. J. C.; Hamley, I. W., Peptide nanotubes self-assembled from leucine-rich alpha helical surfactant-like peptides. *Chem. Comm.* **2020,** *56* (80), 11977-11980.

20. Castelletto, V.; Seitsonen, J.; Ruokolainen, J.; Hamley, I. W., Alpha helical surfactant-like peptides self-assemble into pH-dependent nanostructures. *Soft Matter* **2021,** *17* (11), 3096-3104.

21. Micsonai, A.; Wien, F.; Kernya, L.; Lee, Y.-H.; Goto, Y.; Réfrégiers, M.; Kardos, J., Accurate secondary structure prediction and fold recognition for circular dichroism spectroscopy. *Proc. Natl. Acad. Sci. U.S.A.* **2015,** *112* (24), E3095-E3103.

22. Micsonai, A.; Wien, F.; Bulyáki, É.; Kun, J.; Moussong, É.; Lee, Y.-H.; Goto, Y.; Réfrégiers, M.; Kardos, J., BeStSel: a web server for accurate protein secondary structure prediction and fold recognition from the circular dichroism spectra. *Nucleic Acids Res.* **2018,** *46* (W1), W315-W322.

23. Micsonai, A.; Moussong, É.; Wien, F.; Boros, E.; Vadászi, H.; Murvai, N.; Lee, Y.-H.; Molnár, T.; Réfrégiers, M.; Goto, Y.; Tantos, Á.; Kardos, J., BeStSel: webserver for secondary structure and fold prediction for protein CD spectroscopy. *Nucleic Acids Res.* **2022,** *50* (W1), W90-W98.

24. Fujiwara, K.; Toda, H.; Ikeguchi, M., Dependence of α-helical and β-sheet amino acid propensities on the overall protein fold type. *BMC Struct. Biol.* **2012,** *12* (1), 18.

25. Fry, H. C.; Silveira, G. d. Q.; Cohn, H. M.; Lee, B., Diverse Bilayer Morphologies Achieved via α-Helix-to-β-Sheet Transitions in a Short Amphiphilic Peptide. *Langmuir* **2019,** *35* (27), 8961-8967.

26. Solomon, L. A.; Wood, A. R.; Sykes, M. E.; Diroll, B. T.; Wiederrecht, G. P.; Schaller, R. D.; Fry, H. C., Microenvironment control of porphyrin binding, organization, and function in peptide nanofiber assemblies. *Nanoscale* **2019,** *11* (12), 5412-5421.

27. Yang, H.; Yang, S.; Kong, J.; Dong, A.; Yu, S., Obtaining information about protein secondary structures in aqueous solution using Fourier transform IR spectroscopy. *Nat. Protoc.* **2015,** *10* (3), 382-396.

28. Barth, A., Infrared spectroscopy of proteins. *Biochim. Biophys. Acta - Bioenerg.* **2007,** *1767* (9), 1073-1101.

29. Johnson Jr., W. C., Protein secondary structure and circular dichroism: A practical guide. *Proteins: Struct., Funct., Bioinf.* **1990,** *7* (3), 205-214.

30. Miles, A. J.; Wallace, B. A., Circular dichroism spectroscopy of membrane proteins. *Chem. Soc. Rev.* **2016,** *45* (18), 4859-4872.

31. Fry, H. C.; Peters, B. L.; Ferguson, A. L., Pushing and Pulling: A Dual pH Trigger Controlled by Varying the Alkyl Tail Length in Heme Coordinating Peptide Amphiphiles. *J. Phys. Chem. B.* **2021,** *125* (5), 1317-1330.

32. Kuželová, K.; Mrhalová, M.; Hrkal, Z., Kinetics of heme interaction with heme-binding proteins: The effect of heme aggregation state. *Biochim. Biophys. Acta, Gen. Subj.* **1997,** *1336* (3), 497-501.

33. Larsen, R. W., Volume and thermodynamic profiles of CO-binding to Fe(II) protoporphyrin IX in detergent micelles. *Inorg. Chim. Acta.* **1999,** *288* (1), 74-81.

34. Boffi, A.; Das, T. K.; Della Longa, S.; Spagnuolo, C.; Rousseau, D. L., Pentacoordinate hemin derivatives in sodium dodecyl sulfate micelles: model systems for the assignment of the fifth ligand in ferric heme proteins. *Biophys. J.* **1999,** *77* (2), 1143-1149.

35. Yukl, E. T.; Jepkorir, G.; Alontaga, A. Y.; Pautsch, L.; Rodriguez, J. C.; Rivera, M.; Moënne-Loccoz, P., Kinetic and Spectroscopic Studies of Hemin Acquisition in the Hemophore HasAp from Pseudomonas aeruginosa. *Biochemistry* **2010,** *49* (31), 6646-6654.

36. Lukat-Rodgers, G. S.; Correia, C.; Botuyan, M. V.; Mer, G.; Rodgers, K. R., Heme-Based Sensing by the Mammalian Circadian Protein CLOCK. *Inorg. Chem.* **2010,** *49* (14), 6349-6365.

37. Moffet, D. A.; Case, M. A.; House, J. C.; Vogel, K.; Williams, R. D.; Spiro, T. G.; McLendon, G. L.; Hecht, M. H., Carbon Monoxide Binding by de Novo Heme Proteins Derived from Designed Combinatorial Libraries. *J. Am. Chem. Soc.* **2001,** *123* (10), 2109-2115.

38. Gibson, Q.; Ainsworth, S., Photosensitivity of Hæm Compounds. *Nature.* **1957,** *180*, 1416–1417.

39. Whited, C. A.; Warren, J. J.; Lavoie, K. D.; Winkler, J. R.; Gray, H. B., Kinetics of CO recombination to the heme in Geobacillus stearothermophilus nitric oxide synthase. *Polyhedron.* **2013,** *58*, 134-138.

40. Sugimoto, T.; Unno, M.; Shiro, Y.; Dou, Y.; Ikeda-Saito, M., Myoglobin Mutants Giving the Largest Geminate Yield in CO Rebinding in the Nanosecond Time Domain. *Biophys. J.* **1998,** *75* (5), 2188-2194.

41. Solomon, L. A.; Kodali, G.; Moser, C. C.; Dutton, P. L., Engineering the Assembly of Heme Cofactors in Man-Made Proteins. *J. Am. Chem. Soc.* **2014,** *136* (8), 3192-3199.

42. Ghirlanda, G.; Osyczka, A.; Liu, W.; Antolovich, M.; Smith, K. M.; Dutton, P. L.; Wand, A. J.; DeGrado, W. F., De Novo Design of a D2-Symmetrical Protein that Reproduces the Diheme Four-Helix Bundle in Cytochrome bc1. *J. Am. Chem. Soc.* **2004,** *126* (26), 8141-8147.

For Table of Contents Use Only